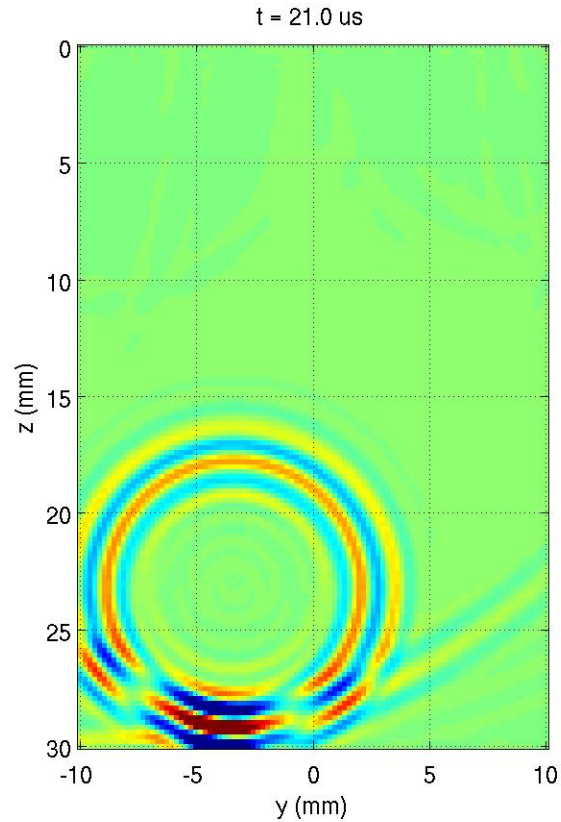## 1. Focused wave and a single scatterer

The pressure field for a focused transmit wave and point target both centered at y = nY/3 and z = nZ/1.3 was simulated in Fullwave. A snapshot of the field corresponding to t = 21 μs of the simulated time vector (where t = 0 after transmission of the first pulse) is shown below.


Fig. 1: Pressure field at t = 21 μs. Note that t = 0 corresponds to the end of the first transmit pulse (i.e. after emission of the first 2-cycle pulse of the focused Tx beam).

2. Propagation in human tissue
a. PSF in homogenous tissue and abdomen

The effects of tissue layers on an ultrasound imaging system were evaluated via comparison of simulated PSFs in homogenous tissue and in a human abdomen phantom.
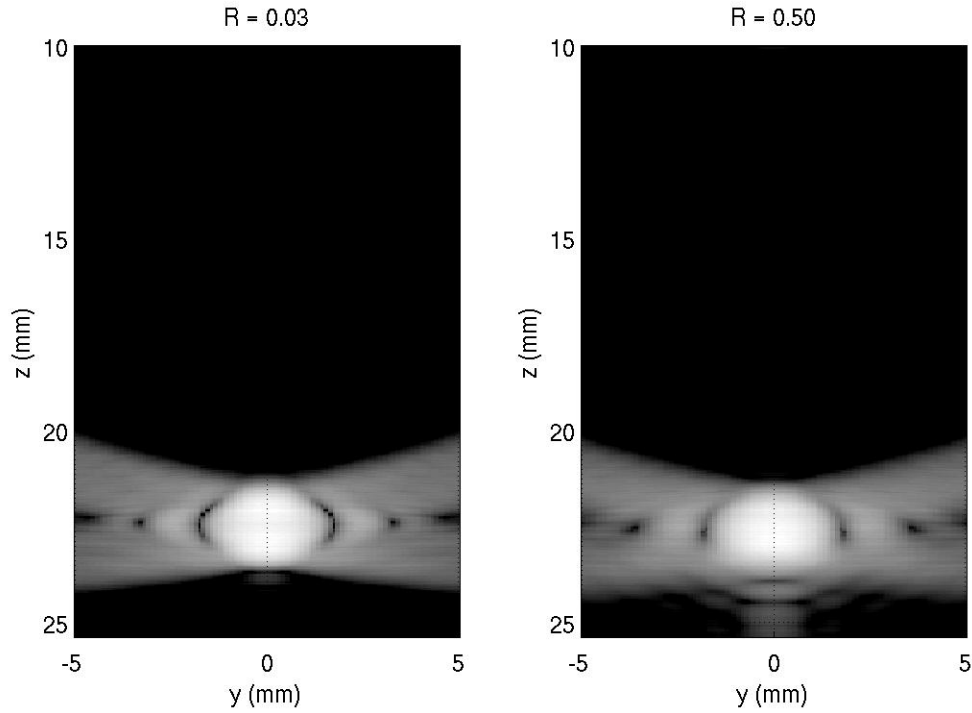
Fig. 2: PSF in homogenous tissue medium generated using point targets with reflection coefficients R = 0.03 and 0.5 at 45 dB dynamic range.

As shown in the figure above, increase in the reflection coefficient from of the scatterer does not significantly alter the PSF in the homogenous condition. Echoes are only generated from the single inhomogeneous point scatterer. Consequently, an increase in the reflection or echo amplitude from this point does not drastically change the log-compressed B-mode image representing the relative echo magnitude of the acoustic field.
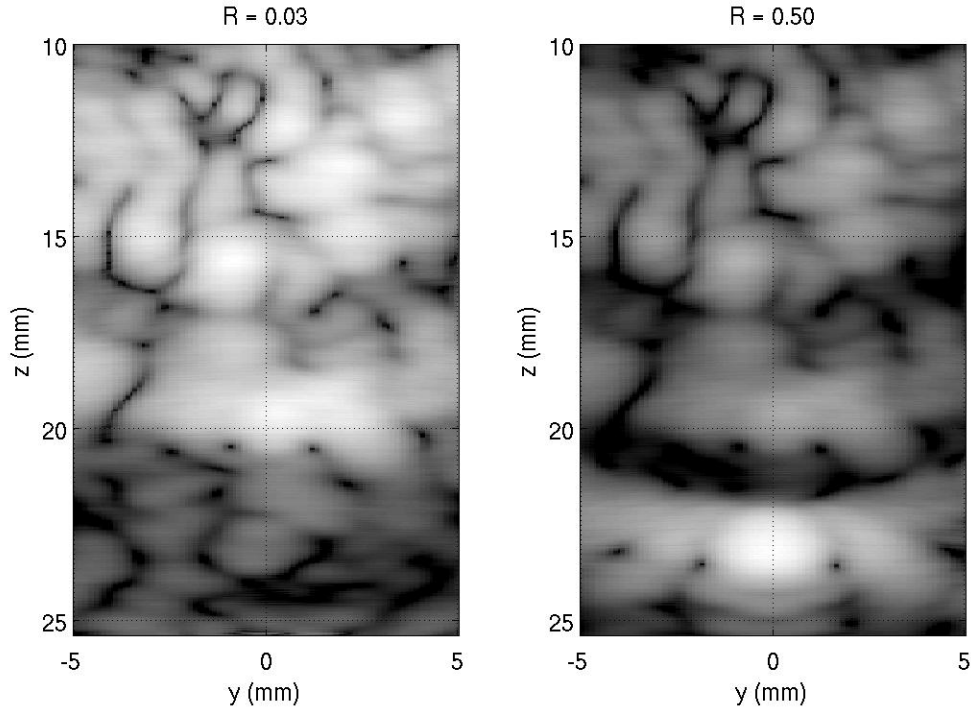
Fig. 3: PSF in tissue medium with aberrating near-field tissue layers generated using point targets with reflection coefficients R = 0.03 and 0.5 at 45 dB dynamic range.

For the human abdomen simulation, there is a notable change in the PSF with increased reflection of the point scatterer. In the presence of tissue layers, reverberation from echoes in the near field tissue layers overwrites the echoes from the point scatterer. For instance, in the R = 0.03 condition, the original PSF profile is completely obscured by noise. With increased reflection coefficient, however, the point scatterer generates a higher amplitude echo relative to the reverberation and clutter from the near field, and as a result, the point target is more easily discerned from the diffuse noise.

b. 1 & 1.5 MHz B-mode images of abdomen

The influence of transmit frequency on image quality was investigated by simulating matched B-mode images using 1 MHz and 1.5 MHz transmit frequencies. It should be noted that Fullwave simulation runtime increases with higher transmit frequency. Maintaining constant points per wavelength (ppw = 15), the 1.5 MHz simulation requires more grid points to analyze the same imaging depth due to shorter wavelengths with increased frequency. Thus, the observed ~2.8 fold increase in runtime from 65.4 s (1 MHz simulation) to 182 s (1.5 MHz simulation) is expected.
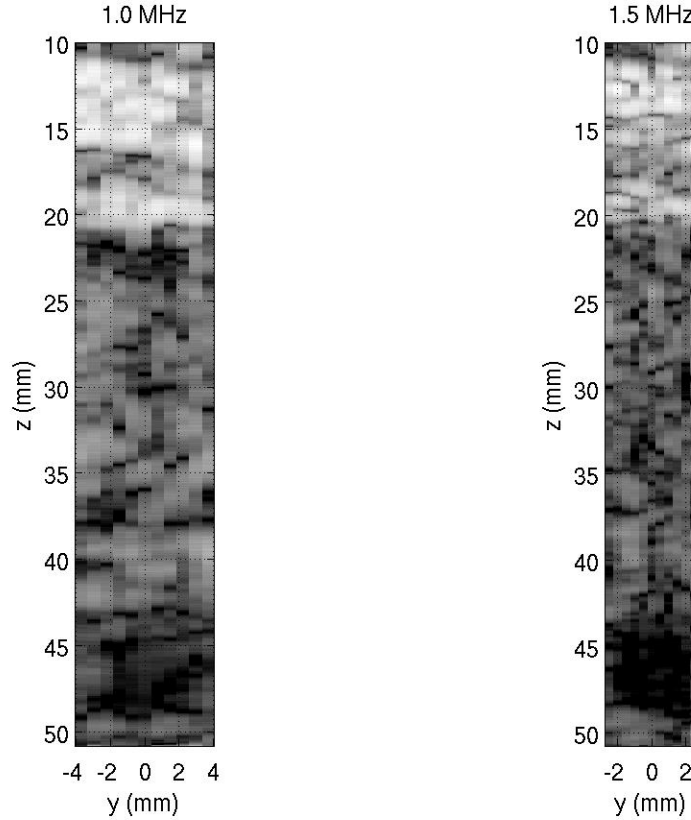
Fig. 4: B-mode images generated using transmit frequency 1.0 MHz (left) and 1.5 MHz (right) shown with 40 dB dynamic range.

B-mode images for the 1 and 1.5 MHz conditions demonstrate clear relationships between image quality and ultrasound frequency. As expected, we observe higher resolution in the 1.5 MHz simulation due to the narrower axial and lateral beam profile generated by the shorter wavelength pulse. This results in notable improvement in the definition of superficial tissue layers as well as the border of the anechoic lesion.

On the other hand, the penetration depth is lower for the 1.5 MHz case. Frequency dependent attenuation leads to greater attenuation of higher frequencies, resulting in lower echo amplitude with propagation. As observed in figure 3, the image generated with 1 MHz transmit frequency maintains more uniform amplitude throughout the imaging depth. The relative effect of attenuation, however, is not severe as simulated depths are relatively shallow and the 0.5 MHz difference between simulated frequencies is small.

Related to this phenomenon, improved lesion contrast is observed in the 1.5 MHz condition. Given the higher attenuation associated with higher transmit frequency, increased lesion contrast may result from more severe attenuation of reverberation from the superficial layers. In the 1 MHz condition, reverberation from these layers is not sufficiently attenuated, resulting in diffuse clutter noise that overwrites echo signals from the anechoic lesion.

3. Harmonic imaging in human tissue
a. Fundamental and harmonic energy versus depth

Using a tissue layer phantom, fundamental and harmonic energies with propagation depth were calculated by windowing the beamformed RF data at various depths, computing the spectra of each window, Gaussian filtering the signals around the fundamental and 2nd harmonic, and integrating both the harmonic and fundamental filtered spectra to find the total energy in each band. Note that for all harmonic simulations, the ppw was set to 20 in order to accurately simulate and accommodate the higher harmonic frequencies. The B/A parameter of the homogenous tissue was set to 8 in order to ensure non-linear wave propagation.
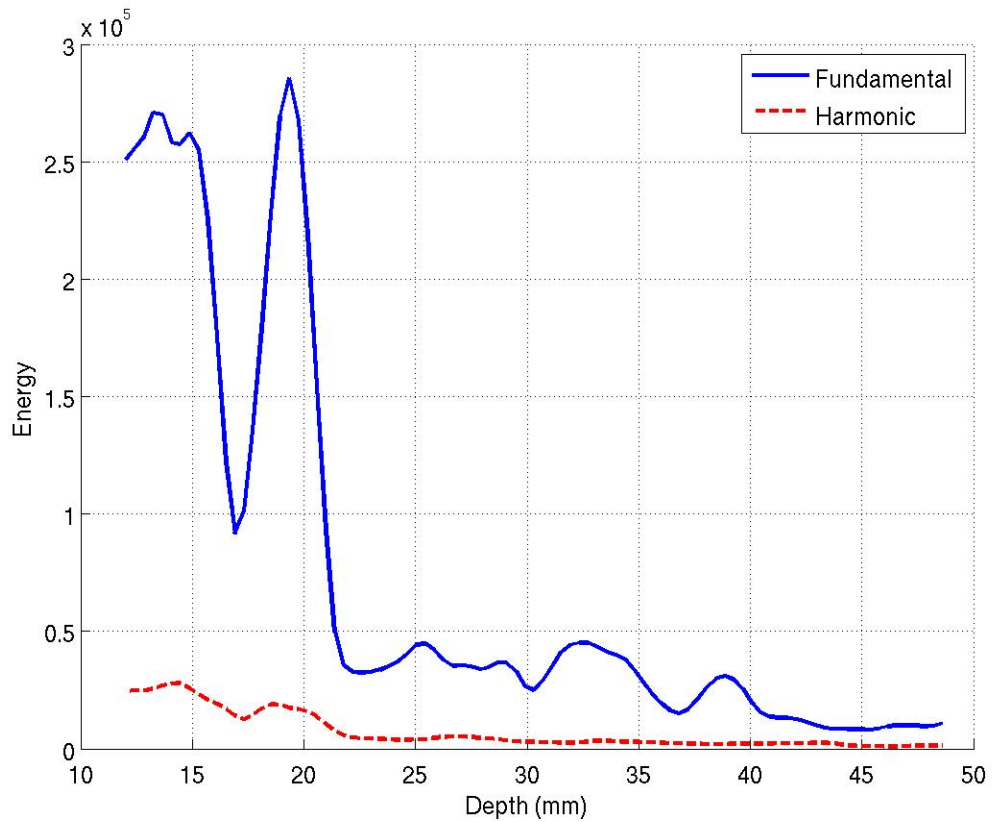
Fig. 5: Fundamental and harmonic energy plotted as a function of depth for ultrasound propagation through the simulated tissue-mimicking layer phantom.
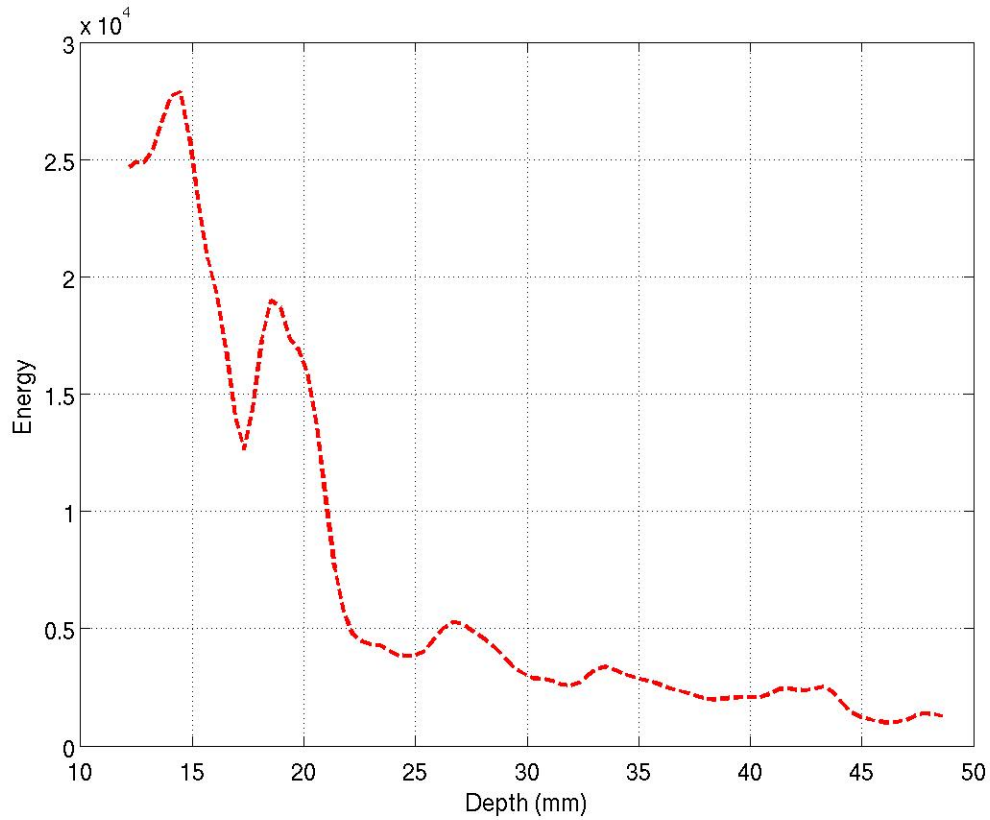
Fig. 6: Harmonic energy plotted alone as a function of depth for ultrasound propagation through the simulated tissue-mimicking layer phantom.

The trends observed in figure 5 can be described by a number of phenomena associated with harmonic and fundamental wave propagation. The initially large fundamental and harmonic energies at lower depths can be attributed to high amplitude backscatter in the near field generated by large impedance mismatches between connective and adipose tissue layers. These high energies in the fundamental and harmonic bands drop off almost immediately at 20 mm where the tissue layer ends. With increased propagation depth, there is a more gradual decrease in both fundamental and harmonic energy which can be related to attenuation. As observed in figure 6, this gradual loss in energy with depth appears to be more severe for the harmonic energies as a result of frequency dependent attenuation. This is highlighted by the notably lower relative amplitude of the energy peak at ~18 mm in the harmonic condition compared to the fundamental condition. At roughly 45 to 50 mm, both fundamental and harmonic energies exhibit a small decrease in energy where the anechoic lesion is located. Though the transmit focus (located at 46 mm) is expected to generate an increase in both fundamental and harmonic energy from focal gain, the presence of the anechoic lesion and absence of scattering media in this region results in decreased backscatter energy.

b. CNR with fundamental and harmonic imaging

Fundamental and harmonic B-mode images of the tissue layer phantom were generated by bandpass filtering the beamformed RF data at the fundamental and second harmonic frequencies, respectively. Using these images, CNR values of the anechoic lesion centered at ~46 mm for each imaging scenario were calculated using the mean and variance of equally sized kernels from inside the lesion and the surrounding uniform tissue.
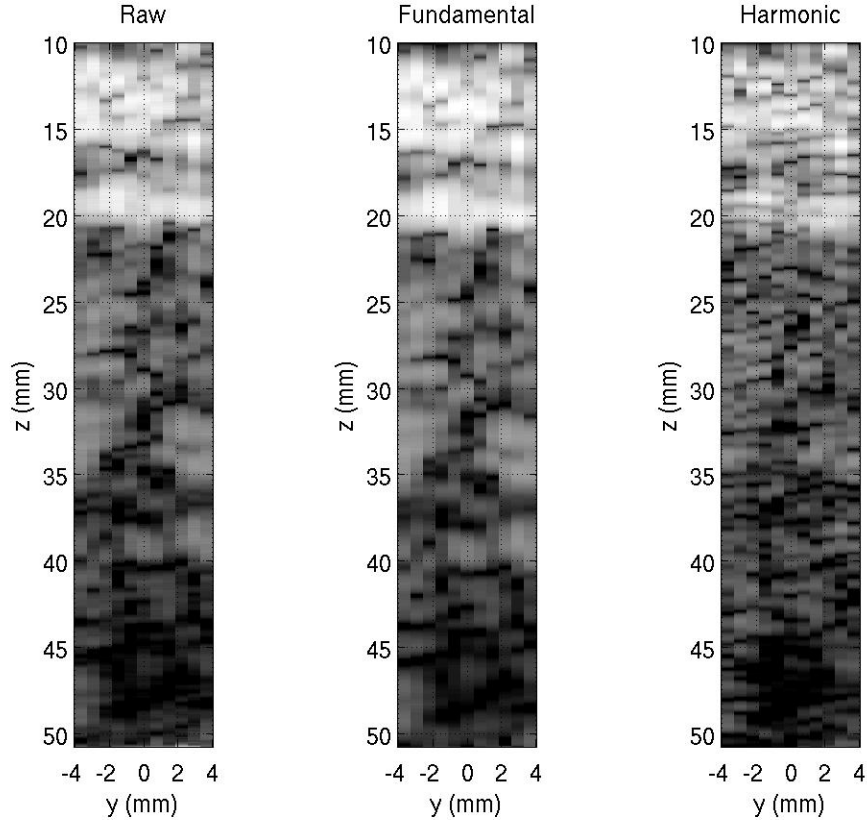
Fig. 7: B-mode images generated using raw RF data, RF data bandpass filtered at the fundamental frequency, and RF data bandpass filtered at the second harmonic frequency.

Table I: Calculated lesion CNR for unfiltered/raw, fundamental, and harmonic imaging

	CNR
Raw	0.95
Fundamental	0.88
Harmonic	1.13

Given the higher frequency band used in harmonic imaging, we observe improved resolution in the harmonic B-mode image. This can be seen in both the superficial tissue layers as well as the lesion boundary. Calculated CNR values as well as comparison of B-mode images furthermore show improvement in anechoic lesion contrast with harmonic imaging. Because harmonics are gradually generated as the beam propagates deeper

through tissue, reflections and reverberation in the near field largely remain at the fundamental frequency. By attenuating the fundamental frequency and using only the harmonic signals, harmonic imaging helps eliminate the high amplitude reverberation echoes from the near field and reduce diffuse clutter in the echo signal in order to improve lesion contrast.

References
[1] G.F. Pinton, J. Dahl, S. Rosenzweig, and G.E. Trahey. A heterogeneous nonlinear attenuating full- wave model of ultrasound. Ultrasonics, Ferroelectrics, and Frequency Control, IEEE Transactions on, 56(3):474–488, March 2009.